



CHORUS

This is the accepted manuscript made available via CHORUS. The article has been published as:

Scanning tunneling spectroscopy study of quasiparticle interference on the dual topological insulator $\text{Bi}_{1-x}\text{Sb}_x$

Shunsuke Yoshizawa, Fumitaka Nakamura, Alexey A. Taskin, Takushi Iimori, Kan Nakatsuji, Iwao Matsuda, Yoichi Ando, and Fumio Komori

Phys. Rev. B **91**, 045423 — Published 20 January 2015

DOI: [10.1103/PhysRevB.91.045423](https://doi.org/10.1103/PhysRevB.91.045423)

Scanning tunneling spectroscopy study of quasiparticle interference on dual topological insulator $\text{Bi}_{1-x}\text{Sb}_x$

Shunsuke Yoshizawa,^{1,*} Fumitaka Nakamura,¹ Alexey A. Taskin,² Takushi Iimori,¹ Kan Nakatsuji,^{1,†} Iwao Matsuda,¹ Yoichi Ando,^{2,‡} and Fumio Komori^{1,§}

¹*Institute for Solid State Physics, The University of Tokyo, Kashiwa, Chiba 277-8581, Japan*

²*Institute of Scientific and Industrial Research, Osaka University, Ibaraki, Osaka 567-0047, Japan*

(Dated: January 6, 2015)

Electronic states of the topological insulator $\text{Bi}_{1-x}\text{Sb}_x$ which is nontrivial in terms of both the Z_2 index and the mirror Chern number, were studied by quasiparticle interference (QPI) using low-temperature scanning tunneling spectroscopy. Our Fourier-transform analysis of the QPI patterns reveals the dispersion of the two surface bands above the Fermi energy (E_F). Absence of the surface band crossing is unambiguously confirmed, which allowed us to elucidate the mirror Chern number of this system is -1 . We also found that Co atoms deposited onto a clean surface of $\text{Bi}_{1-x}\text{Sb}_x$ create impurity states with a clover-leaf-like shape at around 80 meV above E_F . While additional spin-flipping scatterings due to those Co atoms cannot be detected by QPI because of the inherent absence of interference between states with antiparallel spins, we observed clear enhancement of spin-conserving scatterings after Co deposition.

I. INTRODUCTION

Three-dimensional (3D) topological insulators (TIs) are characterized by a nontrivial topological invariant, which is protected by symmetry and the presence of a bulk band gap.^{1,2} So far, two types of topological invariants have been found to be useful for finding 3D TIs.² One is called Z_2 index, which becomes nontrivial when bulk band inversion takes place at an odd number of time-reversal-invariant momenta in the Brillouin zone due to strong spin-orbit coupling; a nontrivial Z_2 topology of the bulk state gives rise to spin-polarized metallic surface states, which are protected by time-reversal symmetry (TRS). The other topological invariant is called mirror Chern number, which is calculated based on the Chern number in each Hilbert subspace divided by the mirror eigenvalue^{3,4}; a nontrivial mirror Chern number defines a 3D topological crystalline insulator (TCI), which is associated with metallic surface states protected by mirror symmetry of the crystal and robust against TRS breaking.^{2,4} Insulators belonging to both of the topological phases may be called “dual” TIs. Bulk $\text{Bi}_{1-x}\text{Sb}_x$ alloy is well known as the first-generation 3D Z_2 TI for $x \sim 0.1-0.2$,^{3,5-9} and this material has actually been predicted to be a dual TI.³ It has three surface-state bands Σ_1 , Σ_2 and Σ'_1 along the $\bar{\Gamma}$ - \bar{M} line of the surface Brillouin zone. Elucidating whether the Σ_1 band crosses the Σ_2 band is crucial for determining the mirror Chern number of this material, which can be either $+1$ or -1 .³ Although the electronic structure of the occupied states in $\text{Bi}_{1-x}\text{Sb}_x$ has been well studied by means of angle-resolved photoemission spectroscopy (ARPES),⁵⁻⁹ the structure of the whole surface bands including the unoccupied states has not been observed in pristine samples. This is because tops of the Σ_1 and Σ_2 bands lie above the Fermi energy, E_F , which is consistent with theoretical calculations.^{3,10} While the top of the Σ_1 band can be shifted below E_F by doping⁶, the Z_2

band has only been inferred from the occupied-state data. To unambiguously elucidate the mirror Chern number of $\text{Bi}_{1-x}\text{Sb}_x$ from the whole band structure, measurements of the quasiparticle interference (QPI) using the Fourier-transform scanning tunneling spectroscopy (FT-STTS) is useful, because the band dispersions of the unoccupied states can be deduced by analyzing the QPI.¹¹⁻¹⁶

Reflecting the spin polarization of the surface states, there is no interference coming from the states with antiparallel spins. This fact allows us to obtain information about the spin texture of the topological surface bands. Magnetic impurity breaks TRS and induces spin-flip scattering among the surface bands. This was demonstrated in Fe-doped Bi_2Se_3 ¹⁷ by QPI, while the effect of deposited magnetic atoms on the surface bands of TIs has not been clearly detected.¹⁸⁻²¹ The $\text{Bi}_{1-x}\text{Sb}_x$ alloy would be suitable for the studies of both the spin texture and the change caused by surface magnetic impurities, because the disorder in the electrostatic potential due to the alloying gives rise to QPI on the pristine surface.¹²

In the present paper, we elucidate the dispersions of the unoccupied electronic states via the analysis of the QPI on the clean cleaved surface of $\text{Bi}_{1-x}\text{Sb}_x$ and unambiguously determine its mirror Chern number to be -1 . We have also studied the surface with deposited Co atoms to explore the possible effects of the magnetic scattering on the electronic states.

II. EXPERIMENTAL METHOD

$\text{Bi}_{1-x}\text{Sb}_x$ ($x = 0.21$) single crystals were grown from stoichiometric mixtures of 99.9999% purity Bi and Sb by the zone-melt method. The samples were cleaved in a vacuum ($\sim 10^{-8}$ Torr) at room temperature to expose the (111) surface and transferred immediately to an ultra-high vacuum (UHV) chamber ($\sim 10^{-10}$ Torr). The FT-STTS technique was used as in the previous stud-

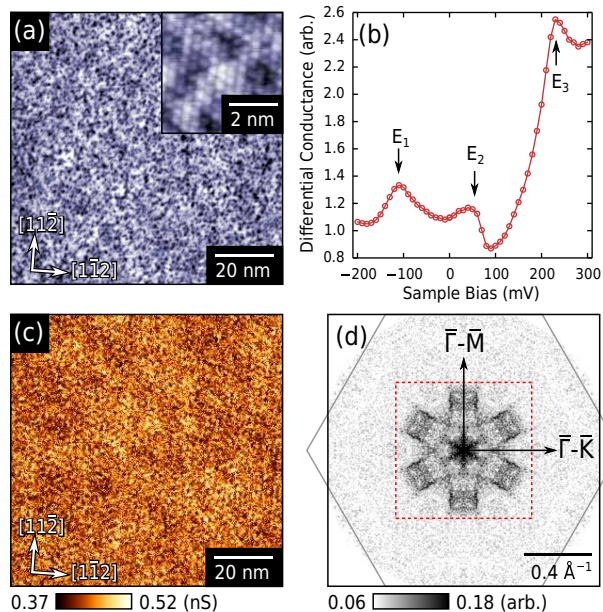


FIG. 1. (Color online) (a) STM image of a $93 \text{ nm} \times 93 \text{ nm}$ region on a clean surface of $\text{Bi}_{1-x}\text{Sb}_x$ obtained at a constant current mode. (Setpoint: 200 pA at 500 mV) The inset shows the close up image of a $5 \text{ nm} \times 5 \text{ nm}$ region revealing the hexagonal lattice of surface atoms. (Setpoint: 500 pA at 500 mV) (b) Average of 256×256 tunneling spectra measured on the same region. The peaks at E_1 , E_2 , and E_3 are the van Hove singularities related to the surface bands. (Bias modulation: $7 \text{ mV}_{\text{rms}}$ at 396 Hz ; Setpoint: 500 pA at 500 mV) (c) Spatial mapping of dI/dV at $+80 \text{ mV}$ of the same region. (d) FT image calculated from the dI/dV in (c). All the equivalent points are averaged to increase signal-to-noise ratio. The hexagon represents the size and the orientation of the surface Brillouin zone. The dashed square represents the area displayed in the FT images in Fig. 2(a)-(d).

ies of Z_2 TIs,^{11–16} and will be described in detail below. The surfaces were studied at 5 K using a low-temperature scanning tunneling microscope (STM) with an electrochemically-etched W tip. Its metallic density of states (DOS) were confirmed on a clean Pt(111) surface. After collecting data on the clean $\text{Bi}_{1-x}\text{Sb}_x$ surfaces, a small amount of Co was deposited at room temperature in UHV. The samples were immediately moved back to the STM kept at 5 K , and spectroscopy measurements were performed in the same way.

III. RESULTS AND DISCUSSION

A. QPI imaging on a clean surface

Figure 1(a) shows a typical STM image on a cleaved surface of the sample. The image displays a nanometer-scale electronic inhomogeneity reflecting the alloying of Bi and Sb as well as the hexagonal atomic lattice (inset).

In this region we measured a tunneling spectrum at each point of 256×256 mesh using a standard lock-in technique. Figure 1(b) shows the averaged tunneling spectrum. Three peaks are noticeable at $E_1 \sim -110 \text{ meV}$, $E_2 \sim +50 \text{ meV}$, and $E_3 \sim +220 \text{ meV}$, and correspond to the van Hove singularities at the maxima of the surface state bands. QPI was observed as spatial modulations in the intensity mappings of dI/dV , as shown in Fig. 1(c). To clarify the periodicity, Fourier transform (FT) images [Fig. 1(d)] were computed from the dI/dV maps. Since the intensity of QPI with long wavevectors is hardly discernible in the present experiment, we focus on the $0.8 \text{ \AA}^{-1} \times 0.8 \text{ \AA}^{-1}$ region inside the dashed square in the following analysis.

Figure 2(a)-(d) shows selected FT images obtained on the clean surface.²² To analyze the energy dependence of these characteristic patterns, we measure line profiles along the $\bar{\Gamma}-\bar{M}$ and $\bar{\Gamma}-\bar{K}$ directions plotted as functions of the length of the wavevector \mathbf{q} and energy E . In Fig. 2(e), the profiles plotted in grayscale reveal several continuous curves reflecting the dispersions of QPI. Figure 2(f) shows the profiles along the dotted line in Fig. 2(c). This measures the separation between the parallel-oriented segments, enclosed by dotted ellipses, observed in the energy range between $+70$ and $+190 \text{ meV}$. In total, 11 dispersing peaks are found, and their positions and the intensities are plotted in Fig. 2(g) and (h).

To relate the observed FT peaks to the surface band structure, we followed the strategies developed in the QPI studies on cuprates,^{23–25} which can be summarized as follows: As the DOS is proportional to the $[\nabla E(\mathbf{k})]^{-1}$ integrated over the Brillouin zone, locations with small $\nabla E(\mathbf{k})$ dominates the QPI formation.²⁴ Such locations correspond to the sharp tips on the contours of the constant energy (CCE). Therefore, the wavevectors of QPI can be associated with the ‘scattering vectors’ connecting two tips on the CCE of the band structure.

Figure 2(j) shows the supposed CCE in the energy range from E_1 to E_2 crossing E_F .^{5–9} The CCE consist of a pocket A at $\bar{\Gamma}$, six pockets B on the $\bar{\Gamma}-\bar{M}$ lines, and six pockets C near \bar{M} . Pockets B originate from the Σ_1 band, while pockets A and C from the Σ_2 band. Previous ARPES studies have revealed another six pockets around \bar{M} ,^{7–9} but their involvement in the QPI observed in the present study is not discernible. The FT profiles in this energy range show three peaks \mathbf{q}_2 , \mathbf{q}_3 , and \mathbf{q}_4 . We can assign \mathbf{q}_2 to a scattering vector connecting pockets A and B, and \mathbf{q}_3 and \mathbf{q}_4 to vectors connecting B pockets. These assignments are the same as those proposed in the previous FT-STs study on $\text{Bi}_{1-x}\text{Sb}_x$ near E_F .¹² These \mathbf{q} vectors increase in length with increasing energy, and vanish at about E_2 . Thus, E_2 is the maximum of the surface band Σ_1 .

In the energy range between E_2 and E_3 , the CCE consist of pockets A and C, as shown in Fig. 2(k). Theoretical calculations¹⁰ show that the inner part of the Σ_2 band moves away from $\bar{\Gamma}$ point faster in $\bar{\Gamma}-\bar{M}$ than in $\bar{\Gamma}-\bar{K}$. This means that the pocket A is warped and be-

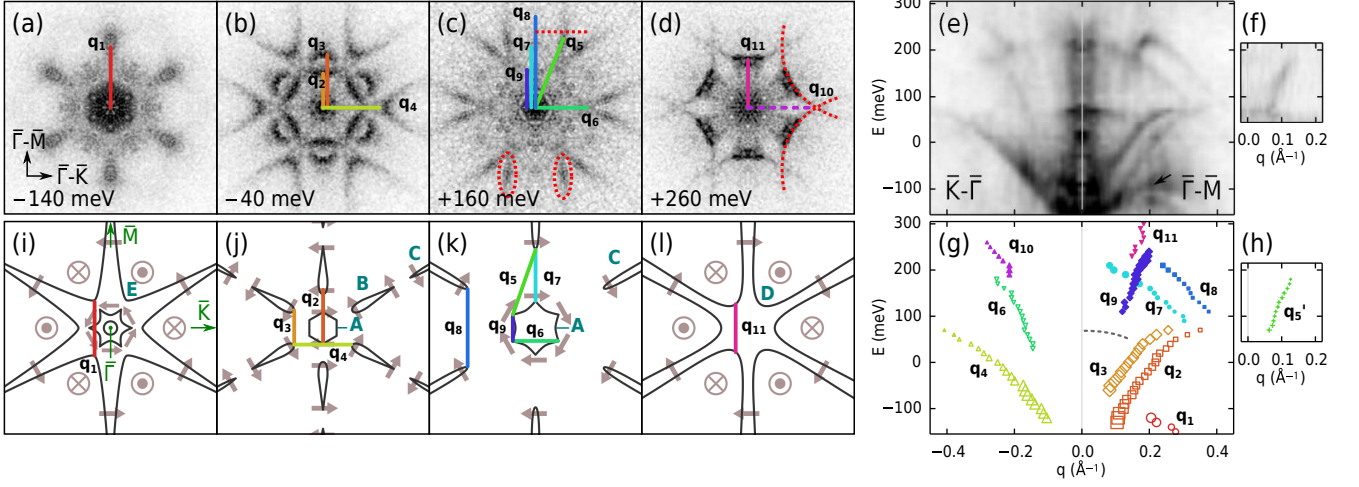


FIG. 2. (Color online) (a)-(d) FT of dI/dV maps at $E = -140, -40, +160,$ and $+260$ meV on a clean surface of $\text{Bi}_{1-x}\text{Sb}_x$. (e) Profiles of the FT images in the $\bar{\Gamma}\text{-}\bar{M}$ and the $\bar{\Gamma}\text{-}\bar{K}$ directions plotted in grayscale. The arrow at around -100 meV in the $\bar{\Gamma}\text{-}\bar{M}$ direction indicate an artifact which disappears in the FT of $(dI/dV)/(I/V)$ maps.²¹ (f) Profiles along the dotted straight line in (c). This shows the dispersion along the $\bar{\Gamma}\text{-}\bar{K}$ of the feature enclosed by dotted ellipses in (c). (g) Peak positions of the FT profiles. The size (area) of each marker is proportional to the peak intensity. Dashed line around 70 meV is a possible FT peak corresponding to QPI within the B pocket, but not analyzed in detail. (h) Peak positions of the profile in (f). (i)-(l) Schematic CCE in the four energy ranges: (i) $E < E_1$, (j) $E_1 < E < E_2$, (k) $E_2 < E < E_3$, and (l) $E_3 < E$. The pockets are labeled by A-E. The scattering vectors corresponding to the observed FT peaks are labeled by $\mathbf{q}_1\text{-}\mathbf{q}_{11}$. \mathbf{q}'_5 in the profile image in (h) denotes the $\bar{\Gamma}\text{-}\bar{K}$ component of the wavevector \mathbf{q}_5 . Dotted curves in (d) indicate the tails of the spot labeled by \mathbf{q}_{11} and \mathbf{q}_{10} corresponds to the intersection of the two tails.

comes star-shaped. The FT image indicates five vectors, $\mathbf{q}_5, \mathbf{q}_6, \dots, \mathbf{q}_9$. They can be assigned to vectors connecting the six tips of the warped A pocket and six C pockets, as illustrated in Fig. 2(k). All of these wavevectors disappear at around E_3 , and thus the Σ_2 band has the maximum at E_3 .

Above E_3 , the electron pockets A and C are merged and create six large hole pockets labeled D [Fig. 2(l)]. The FT peak \mathbf{q}_{11} can be assigned to the 120° scattering in the $\bar{\Gamma}\text{-}\bar{M}$ direction between the tips of these pockets, and \mathbf{q}_{10} to the ‘tail’ of the interference pattern of \mathbf{q}_{11} as depicted in Fig. 2(d). Below E_1 , the CCE have two pockets at $\bar{\Gamma}$ and six pockets E in the $\bar{\Gamma}\text{-}\bar{K}$ direction [Fig. 2(i)]. The FT peak in this energy range corresponds to the vector along the $\bar{\Gamma}\text{-}\bar{M}$ direction connecting E pockets.

In these two energy ranges, QPI peaks from 60° scatterings between the neighboring D pockets or E pockets were not observed. This can be understood if we suppose an out-of-plane spin component changing its sign every 60° as in the case of the surface band of $\text{Bi}(111)$ studied by ARPES.²⁶ Here, the spins of neighboring pockets can be almost anti-parallel as depicted in Figs. 2(i) and (l), and QPI due to them should be suppressed.

Using the simple relations between the QPI wavevectors (\mathbf{q}) and momenta of tips in CCE (\mathbf{k}) in Table I, we can now reconstruct the band dispersion from the QPI data. The result is shown in Fig. 3(a). The momenta calculated from different \mathbf{q} vectors fall onto two curves of corresponding to Σ_1 and Σ_2 in the $\bar{\Gamma}\text{-}\bar{M}$ direction, and Σ_3 and Σ_4 in the $\bar{\Gamma}\text{-}\bar{K}$ direction. Below E_F , the

E	$\bar{\Gamma}\text{-}\bar{K}$	$\bar{\Gamma}\text{-}\bar{M}$
$E_3 < E$	$k_{11} = (1/\sqrt{3})q_{11}$	
$E_2 < E < E_3$		$k_9 = q_9$ $k_8 = q_8$ $k_7 = q_7 + q_9$ $k_6 = (1/\sqrt{3})q_6$ $k_5 = (2/\sqrt{3})q'_5$
$E_1 < E < E_2$	$k'_2 = (1/\sqrt{3})k_2$ $k_4 = (\sqrt{3}/2)q_4$ $k_3 = q_3$	$k_4 = (\sqrt{3}/2)q_4$ $k_2 = q_2 - q_3$
$E < E_1$	$k_1 = (1/\sqrt{3})q_1$	

TABLE I. Positions of tips in CCE, k_j , defined as functions of the lengths of QPI wavevectors, $q_i = |\mathbf{q}_i|$. ($i, j = 1, \dots, 11$.) In the energy range between E_1 and E_2 , the pocket A can be approximated by a regular hexagon. Hence we can estimate k'_2 in the $\bar{\Gamma}\text{-}\bar{K}$ direction from k_2 in the $\bar{\Gamma}\text{-}\bar{M}$ direction.

reconstructed band dispersions are consistent with those determined from the ARPES on the $\text{Bi}_{1-x}\text{Sb}_x$ sample with the same Sb concentration.⁹ The maxima of Σ_1 , Σ_2 , and Σ_4 agrees well with the peaks in the tunneling spectrum shown in Fig. 1(b). The internal consistency supports the validity of the present analysis. The absence of the band crossing between Σ_1 and Σ_2 allows us to conclude that the mirror Chern number of $\text{Bi}_{1-x}\text{Sb}_x$ is -1 . This conclusion agrees with the inference derived from the spin polarization of the occupied surface bands,

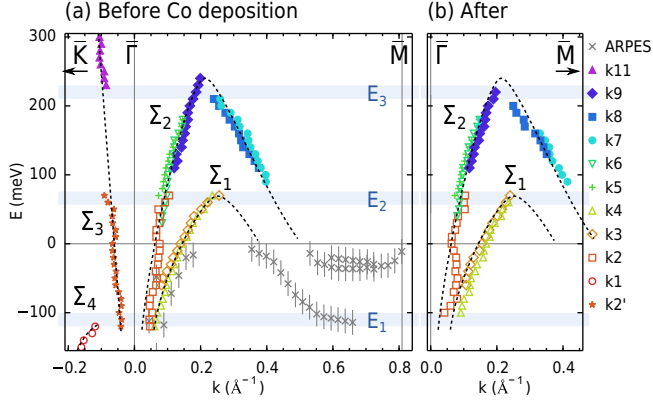


FIG. 3. (Color online) (a) Surface band structure of the clean surface of $\text{Bi}_{1-x}\text{Sb}_x$ reconstructed from our QPI data. Previous ARPES data⁹ with an energy resolution of 18 meV are also plotted. The dashed curves are the guide to the eye. (b) Surface band structure of the same sample after the deposition of Co. The dashed curves same as those in (a) are drawn.

which was measured by spin-resolved ARPES.⁶⁻⁸

B. Effects of Co atoms on the surface states

To search for the effects of magnetic scattering on the helical surface bands, we deposited a small amount of Co on the cleaved surface studied above. Figure 4(a) shows an STM image after the Co deposition. It is nearly indistinguishable from the image obtained on the clean surface [see Fig. 1(a)]. No protrusions that could be assigned to the Co adatoms or clusters were found on the surface. Nonetheless, dI/dV maps and STM images taken at around +80 meV show clover-leaf-like features distributed randomly as in Fig. 4(b). The number of these features (75 in this area) corresponds to 0.2% of the density of surface Bi/Sb atoms. These features are absent on the clean surface and attributed to Co-induced states. The Co atoms are likely to be situated below the surface, because the STM images show no signature of adatoms. Figure 4(c) shows the tunneling spectra measured across one of the clover-leaf-like features. There is a peak at about 70 mV in the tunneling spectrum at the center of this feature. Note that this peak energy slightly depends on the impurity site. Upon moving away from the impurity center, the peak gradually shifts toward lower energies. The spectral shape is not a Fano-type²⁷ indicative of the Kondo resonance²⁸, which quenches the local moment of a magnetic impurity. Because of the absence of the Kondo effect, we suppose the Co atoms still have a magnetic moment at the surface of $\text{Bi}_{1-x}\text{Sb}_x$.

The QPI on this surface was observed and analyzed in the same manner as on the clean surface. Figure 4(d) shows the FT profiles along $\bar{\Gamma}$ - \bar{M} and $\bar{\Gamma}$ - \bar{K} directions. The position and intensity of the FT peaks related to QPI are

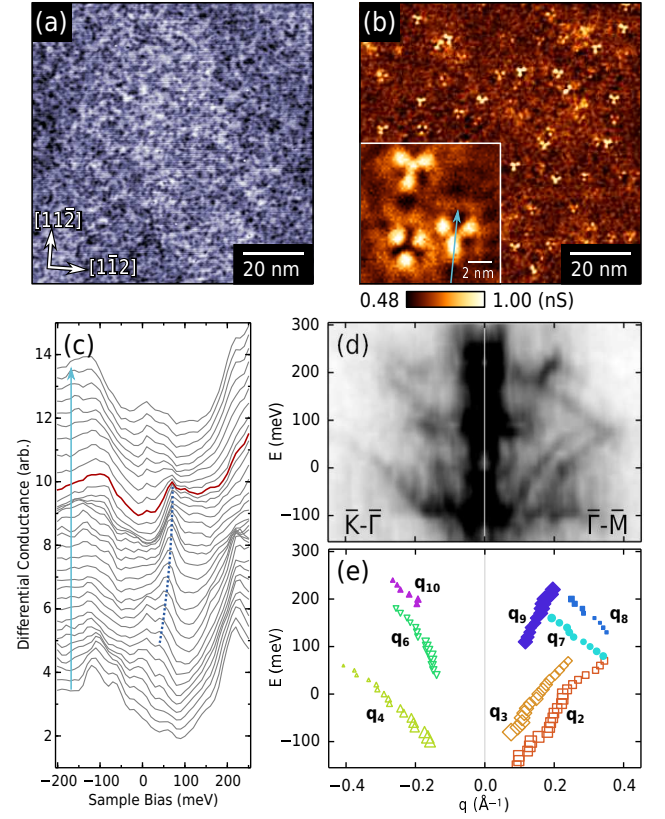


FIG. 4. (Color online) (a) STM image of a $93 \text{ nm} \times 93 \text{ nm}$ region of $\text{Bi}_{1-x}\text{Sb}_x$ after depositing a small amount of Co. (Setpoint: 500 pA at 500 mV) (b) dI/dV map at +80 meV of the same region as (a). The inset shows dI/dV map of a $12 \text{ nm} \times 12 \text{ nm}$ on the same surface. (Bias modulation: 7 mV_{rms} at 396 Hz; Setpoint: 500 pA at 500 mV) (c) Tunneling spectra obtained across one of the clover-leaf-like impurity states. The measurement locations are indicated by the arrow in (c). The thick curve is the spectrum at the center of the clover-leaf-like shape. (d) FT profiles of dI/dV maps after the Co deposition. (e) Position and intensity of FT peaks. The area of each marker is proportional to the peak intensity.

plotted in Fig. 4(e). The observed peak positions are the same as those on the clean surface; nevertheless, the intensities of the \mathbf{q}_6 , \mathbf{q}_7 , and \mathbf{q}_9 peaks became stronger compared to those on the clean surface shown in Fig. 2(g). This means that the Co atoms enhance scatterings of the surface electrons. The energy range where we detected Co-induced states and the enhancement of QPI intensity corresponds roughly to the bulk band gap.^{3,29} In the other energy ranges, the bulk states could be involved in the scattering processes by the Co atoms and make the enhancement of QPI among surface states unremarkable. We note that the absence of additional QPI related to states with anti-parallel spins does *not* mean the absence of magnetic scatterings, because electrons with anti-parallel spins cannot interfere with each other and hence do not give rise to QPI.³⁰⁻³²

The band dispersions reconstructed from the measured

positions of the FT peaks on the Co-deposited surface are shown in Fig. 3(b). The band structure around the $\bar{\Gamma}$ point is essentially unchanged. If the spins of Co atoms are oriented randomly, they do not break mirror symmetry and a transition from a dual TI to a TCI could be realized. The present results suggest that, even in this case, no change in the surface band dispersions would occur except for the region near the \bar{M} points, where the topological surface band Σ'_1 exists but was not probed in the present study. FT-STs with improved experimental conditions would be necessary for probing the electronic states near the \bar{M} points to observe the anticipated transition. This challenge is left for future studies.

IV. CONCLUSIONS

In conclusion, we have studied the surface states of the dual TI $\text{Bi}_{1-x}\text{Sb}_x$ through FT-STs to probe QPI.

Our analysis revealed the band dispersions of the unoccupied surface states. The absence of band crossing between Σ_1 and Σ_2 was unambiguously elucidated, which allowed us to determine the mirror Chern number to be -1 . Co atoms deposited onto a clean surface lead to the appearance of clover-leaf-like impurity states at around 80 meV above E_F . The surface band dispersions were nearly unchanged after the Co deposition, but an enhancement of spin-conserving scatterings was detected through stronger QPI peaks in the FT spectrum.

ACKNOWLEDGMENTS

This work was partly supported by JSPS (KAKENHI Grants No. 26287061 and No. 25220708), by MEXT (Innovative Area “Topological Quantum Phenomena”), and by AFOSR (AOARD 124038).

-
- * Present address: International Center for Materials Nanoarchitectonics, National Institute for Materials Science, 1-1 Namiki, Tsukuba 305-0044, Japan
- † Present address: Department of Materials Science and Engineering, Tokyo Institute of Technology, J1-3, 4259 Nagatsuta-cho, Midori-ku, Yokohama 226-8502, Japan
- ‡ y_ando@sanken.osaka.u.ac.jp
- § komori@issp.u-tokyo.ac.jp
- 1 M. Z. Hasan and C. L. Kane, *Rev. Mod. Phys.* **82**, 3045 (2010).
 - 2 Y. Ando, *J. Phys. Soc. Jpn* **82**, 102001 (2013).
 - 3 J. C. Y. Teo, L. Fu, and C. L. Kane, *Phys. Rev. B* **78**, 045426 (2008).
 - 4 L. Fu, *Phys. Rev. Lett.* **106**, 106802 (2011).
 - 5 D. Hsieh, D. Qian, L. Wray, Y. Xia, Y. S. Hor, R. J. Cava, and M. Z. Hasan, *Nature* **452**, 970 (2008).
 - 6 D. Hsieh, Y. Xia, L. Wray, D. Qian, A. Pal, J. H. Dil, J. Osterwalder, F. Meier, G. Bihlmayer, C. L. Kane, Y. S. Hor, R. J. Cava, and M. Z. Hasan, *Science* **323**, 919 (2009).
 - 7 A. Nishide, A. A. Taskin, Y. Takeichi, T. Okuda, A. Kakizaki, T. Hirahara, K. Nakatsuji, F. Komori, Y. Ando, and I. Matsuda, *Phys. Rev. B* **81**, 041309 (2010).
 - 8 A. Nishide, Y. Takeichi, T. Okuda, A. A. Taskin, T. Hirahara, K. Nakatsuji, F. Komori, A. Kakizaki, Y. Ando, and I. Matsuda, *New J. Phys.* **12**, 065011 (2010).
 - 9 F. Nakamura, Y. Kousa, A. A. Taskin, Y. Takeichi, A. Nishide, A. Kakizaki, M. D’Angelo, P. Lefevre, F. Bertran, A. Taleb-Ibrahimi, F. Komori, S.-i. Kimura, H. Kondo, Y. Ando, and I. Matsuda, *Phys. Rev. B* **84**, 235308 (2011).
 - 10 H.-J. Zhang, C.-X. Liu, X.-L. Qi, X.-Y. Deng, X. Dai, S.-C. Zhang, and Z. Fang, *Phys. Rev. B* **80**, 085307 (2009).
 - 11 S. Kim, S. Yoshizawa, Y. Ishida, K. Eto, K. Segawa, Y. Ando, S. Shin, and F. Komori, *Phys. Rev. Lett.* **112**, 136802 (2014).
 - 12 P. Roushan, J. Seo, C. V. Parker, Y. S. Hor, D. Hsieh, D. Qian, A. Richardella, M. Z. Hasan, R. J. Cava, and A. Yazdani, *Nature* **460**, 1106 (2009).

- 13 T. Zhang, P. Cheng, X. Chen, J.-F. Jia, X. Ma, K. He, L. Wang, H. Zhang, X. Dai, Z. Fang, X. Xie, and Q.-K. Xue, *Phys. Rev. Lett.* **103**, 266803 (2009).
- 14 Z. Alpichshev, J. G. Analytis, J.-H. Chu, I. R. Fisher, Y. L. Chen, Z. X. Shen, A. Fang, and A. Kapitulnik, *Phys. Rev. Lett.* **104**, 016401 (2010).
- 15 M. Nurmamat, E. E. Krasovskii, K. Kuroda, M. Ye, K. Miyamoto, M. Nakatake, T. Okuda, H. Namatame, M. Taniguchi, E. V. Chulkov, K. A. Kokh, O. E. Tereshchenko, and A. Kimura, *Phys. Rev. B* **88**, 081301 (2013).
- 16 W. Ko, I. Jeon, H. W. Kim, H. Kwon, S.-J. Kahng, J. Park, J. S. Kim, S. W. Hwang, and H. Suh, *Sci. Rep.* **3**, 2656 (2013).
- 17 Y. Okada, C. Dhital, W. Zhou, E. D. Huemiller, H. Lin, S. Basak, A. Bansil, Y.-B. Huang, H. Ding, Z. Wang, S. D. Wilson, and V. Madhavan, *Phys. Rev. Lett.* **106**, 206805 (2011).
- 18 M. Ye, S. V. Eremeev, K. Kuroda, E. E. Krasovskii, E. V. Chulkov, Y. Takeda, Y. Saitoh, K. Okamoto, S. Y. Zhu, K. Miyamoto, M. Arita, M. Nakatake, T. Okuda, Y. Ueda, K. Shimada, H. Namatame, M. Taniguchi, and A. Kimura, *Phys. Rev. B* **85**, 205317 (2012).
- 19 T. Valla, Z.-H. Pan, D. Gardner, Y. S. Lee, and S. Chu, *Phys. Rev. Lett.* **108**, 117601 (2012).
- 20 M. R. Scholz, J. Sánchez-Barriga, D. Marchenko, A. Varykhalov, A. Volykhov, L. V. Yashina, and O. Rader, *Phys. Rev. Lett.* **108**, 256810 (2012).
- 21 J. Honolka, A. A. Khajetoorians, V. Sessi, T. O. Wehling, S. Stepanow, J.-L. Mi, B. B. Iversen, T. Schlenk, J. Wiebe, N. B. Brookes, A. I. Lichtenstein, P. Hofmann, K. Kern, and R. Wiesendanger, *Phys. Rev. Lett.* **108**, 256811 (2012).
- 22 The FT images were made from the dI/dV images normalized by I/V .³³ While this process eliminates some artifacts and makes FT images sharp, it reduces the intensity of QPI signals near E_F at the same time. Thus we use FT of dI/dV without this normalization for plotting and analyzing the FT profiles.

- ²³ J. E. Hoffman, K. McElroy, D.-H. Lee, K. M. Lang, H. Eisaki, S. Uchida, and J. C. Davis, *Science* **297**, 1148 (2002).
- ²⁴ K. McElroy, R. W. Simmonds, J. E. Hoffman, D.-H. Lee, J. Orenstein, H. Eisaki, S. Uchida, and J. C. Davis, *Nature* **422**, 592 (2003).
- ²⁵ T. Hanaguri, Y. Kohsaka, J. C. Davis, C. Lupien, I. Yamada, M. Azuma, M. Takano, K. Ohishi, M. Ono, and H. Takagi, *Nature Physics* **3**, 865 (2007).
- ²⁶ A. Takayama, T. Sato, S. Souma, and T. Takahashi, *Phys. Rev. Lett.* **106**, 166401 (2011).
- ²⁷ U. Fano, *Phys. Rev.* **124**, 1866 (1961).
- ²⁸ V. Madhavan, W. Chen, T. Jamneala, M. F. Crommie, and N. S. Wingreen, *Science* **280**, 567 (1998).
- ²⁹ B. Lenoir, A. Dauscher, X. Devaux, R. Martin-Lopez, Y. Ravich, H. Scherrer, and S. Scherrer, *15th International Conference on Thermoelectrics*, , 1 (1996).
- ³⁰ Q. Liu, X.-L. Qi, and S.-C. Zhang, *Phys. Rev. B* **85**, 125314 (2012).
- ³¹ H. Beidenkopf, P. Roushan, J. Seo, L. Gorman, I. Drozdov, Y. S. Hor, R. J. Cava, and A. Yazdani, *Nature Phys.* **7**, 939 (2011).
- ³² A. Stróżecka, A. Eiguren, and J. I. Pascual, *Phys. Rev. Lett.* **107**, 186805 (2011).
- ³³ R. Feenstra, J. A. Stroscio, and A. Fein, *Surf. Sci.* **181**, 295 (1987).